Supporting Information

Energy and Charge Transfer Cascade in Methylammonium Lead Bromide Perovskite Nanoparticle Aggregates

Marine E. F. Bouduban, Andrés Burgos-Caminal, Rachele Ossola, Joël Teuscher, and Jacques-E. Moser*

Photochemical Dynamics Group, Institute of Chemical Sciences & Engineering, and Lausanne Centre for Ultrafast Science (LACUS), École polytechnique fédérale de Lausanne, CH-1015 Lausanne, Switzerland

*E-mail : je.moser@epfl.ch

S1. Complement to Figure 2: Transient absorption spectrum

Fig. S1 displays the transient absorption spectra obtained upon laser pulsed excitation of the colloid at λ_{ex} = 480 nm. Data for λ_{ex} = 390 nm excitation are provided by Fig. 2 in the main text. The oscillatory feature observed in Fig. 2 for λ_{obs} < 500 nm is much weaker here and overlaps with a stronger positive absorbance change peaking at λ_{obs} = 438 nm.

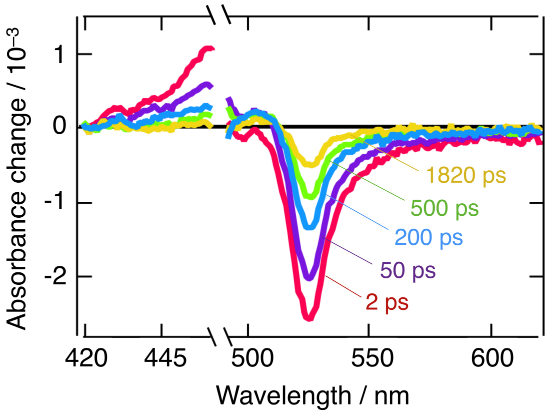

Fig. S1 Transient absorbance spectra for λ_{ex} = 480 nm and time delays ranging from t = 2 ps to 1820 ps. Red : t = 2 ps, purple : 20 ps, blue : 50 ps, green : 500 ps, and yellow : 1820 ps.

S2. Complement to Figure 3: Spectral data and dynamics

Fig. 3 appearing in the main text aims at supporting the hypothesis of interactions between perovskite nanostructures. In this respect, we present two global fits arising from multi-exponential fitting of datasets obtained with $\lambda_{ex} = 390$ nm and $\lambda_{ex} = 480$ nm, respectively. Fig. S2 features the corresponding spectral data and biexponential kinetic fits to support the accuracy of the global fits.

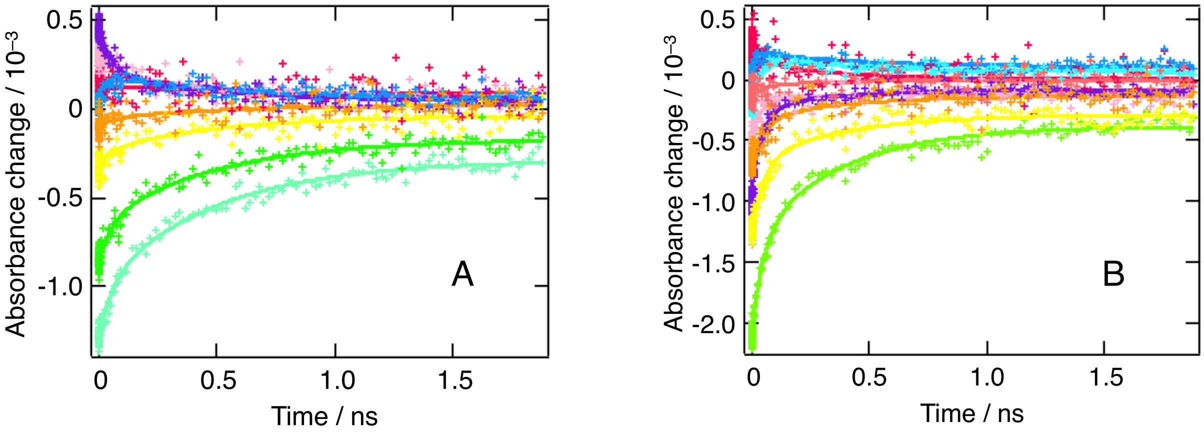

Fig. S2 Examples of global fit results. A) λ_{ex} = 480 nm (markers) fitted with a biexponential kinetic equation (bold lines). Red : λ_{obs} = 430 nm, pink: 450 nm, purple: 460 nm, blue: 500 nm, turquoise: 520 nm, green: 530 nm, yellow: 540 nm, and orange: 560 nm. B) λ_{ex} = 390 nm (markers) fitted with a triexponential function (bold lines). Red : λ_{obs} = 420 nm, pink: 430 nm, purple: 450 nm, blue: 470 nm, green: 490 nm, turquoise: 480 nm, yellow: 520 nm, dark red: 540 nm, orange: 530 nm, and dark pink: 580 nm.

S2. Fitting of kinetic equations

Dynamic traces were fitted with multi-exponential functions, convoluted with a Gaussian instrument response function (IRF) when needed. Datasets reported in Figs 3A and 3B span a time window between $t = 1$ ps and 1880 ps. As a consequence, no convolution with the IRF was needed (Gaussian IRF with $FWHM = 90$ fs for λ_{ex}=480 nm, $FWHM$ =200 fs for λ_{ex}=390 nm).

a) Bi-exponential function:

$$\Delta A(\lambda,\, t) = A_0 + A_1(\lambda)\cdot \exp\left(\frac{-t}{\tau_1}\right) + A_2(\lambda)\cdot \exp\left(\frac{-t}{\tau_2}\right) \tag{S1}$$

b) Tri-exponential function:

$$\Delta A(\lambda,\, t) = A_0 + A_1(\lambda)\cdot \exp\left(\frac{-t}{\tau_1}\right) + A_2(\lambda)\cdot \exp\left(\frac{-t}{\tau_2}\right) + A_3(\lambda)\cdot \exp\left(\frac{-t}{\tau_3}\right) \tag{S2}$$

Ultrafast photoemission data (Fig. 4B) were fitted with a tri-exponential function convoluted with a Gaussian IRF with $FWHM$ =200 fs (λ_{ex} =390 nm: [1]

$$\Delta A(\lambda,\, t) = \frac{1}{2}\sum_{i=1}^{3} \mathrm{y}_i(\lambda)\cdot \exp\left[\frac{\mu - t}{\tau_i} + \frac{1}{2}\left(\frac{\sigma}{\tau_i}\right)^2\right]\cdot\left[1 + erf\left\{\frac{t - \left(\mu + \frac{\sigma^2}{\tau_i}\right)}{\sqrt{2}\cdot\sigma}\right\}\right] \tag{S3}$$

where μ represents the time-origin of the IRF and σ its width, with $FWHM = 2\sigma\cdot\sqrt{2\cdot\ln 2}$.

TCSPC dynamics did not need to be deconvoluted for instrument response function and were fitted with a a simple tri-exponential function:

$$I(t) = a\cdot \exp\left(\frac{-t}{\tau_1}\right) + b\cdot \exp\left(\frac{-t}{\tau_2}\right) + c\cdot \exp\left(\frac{-t}{\tau_3}\right) \tag{S4}$$

S3. Global fitting procedure

Global fits of transient absorbance data have been used in this work to assess the presence of interstructure interactions. A comprehensive review of global analysis can be found elsewhere,[1] and an illustration of the particular case of transient absorption spectra can be found in reference [2].

To perform a global fit, data must first be sampled, and an appropriate number of kinetic traces must be extracted. Then, the point is to apply a kinetic model, usually multi-exponential, where all the traces are forced to evolve with the same time constant(s). This yields the following point by point procedure:

1) Extraction of kinetic traces every 10 nm, between λ_{obs} = 420 and 600 nm.
2) Individual fitting of a few sampled traces to obtain (i) an accurate fitting equation and (ii) a good initial guess for the global fit (faster convergence).
3) Performing of the global fit:
    a. Select the best fitting function (from step 2).
    b. Link the time constant(s) for all the kinetic traces included.
    c. Fill up fitting coefficients for each trace according to the guesses obtained in step 2.
    d. Perform fit with a reasonable number of iterations (typically 40):
        i. If convergence is reached: assess fit quality with the calculated residuals.
        ii. If convergence is not reached: readjust initial guesses and repeat.
4) Extraction of the amplitude coefficient(s) for each trace into new sets of data (one set per coefficient, ie. per exponential). In our case: A_1 and A_2 for λ_{ex} = 480 nm and A_1, A_2 and A_3 for λ_{ex} = 390 nm.
5) Plotting of the constituted amplitude datasets versus wavelengths.

S4. Electroabsorption contribution to transient spectra

The oscillatory feature observed in the transient absorption spectra below 500 nm (Fig. 2) is believed to be due to a photoinduced electroabsorption effect. Separation of photogenerated carrier pairs localized in perovskite nanoparticles indeed submits the material contained between an electron and a hole to an electric field that affects its absorption spectrum. The absorbance change at a particular wavelength can be shown to be quadratic in the field intensity, in accordance with the Stark or Franz-Keldysh-Aspnes theories.[3]

The analysis of the spectral shape of the electroabsorption feature allows to draw important conclusions on the kind of carrier pairs at the origin of the effect. In the frame of the perturbation theory, the differential electroabsorption (EA) signal can be described by the perturbative expansion in the field:[4]

$$\Delta A(\lambda) = -\frac{\partial A(\lambda)}{\partial \lambda}\cdot \boldsymbol{m}_{0k}\cdot \boldsymbol{E} - \frac{1}{2}\cdot\frac{\partial A(\lambda)}{\partial \lambda}\cdot \boldsymbol{p}_{0k}\cdot \boldsymbol{E}^2 + \frac{1}{2}\cdot\frac{\partial^2 A(\lambda)}{\partial \lambda^2}\cdot \boldsymbol{m}_{0k}^2\cdot \boldsymbol{E}^2 + \ldots \qquad \text{(S5)}$$

where $A(\lambda)$ is the absorbance at the wavelength λ, $\boldsymbol{E}$ the applied electric field, and $\boldsymbol{m}_{0k}$ and $\boldsymbol{p}_{0k}$ respectively the change in the permanent dipole moment and the change in the polarizability upon the transition of interest (0 → k). Note that the first term (linear in the field) is expected to cancel out for an isotropic material, such as the perovskite contained in our colloidal suspensions.

As it clearly emerges from Eq. S5, the electroabsorption signal can be decomposed in a linear combination of first and second derivatives of the linear absorption spectrum $A(\lambda)$. The second and third terms of the expansion are quadratic in the field and do not cancel out in an isotropic material. The amplitude of the second derivative contribution is provided by the change in permanent dipole moment $\boldsymbol{m}_{0k}$ of the material and is a direct probe of the presence of CT excitons among the photogenerated species.

Fig. S3A displays the linear absorption spectrum of a suspension of $CH_3NH_3PbBr_3$ nanoparticle aggregates, along with its calculated first and second derivatives. A linear combination of both contributions $S(\lambda)$ defined by Eq. S6, which constitutes a best fit of the transient absorption spectrum recorded at a time delay of 2 ps (Fig. S3B), is also plotted on the same graph.

$$S(\lambda) = 1\cdot\frac{\partial A(\lambda)}{\partial \lambda} + 10\cdot\frac{\partial^2 A(\lambda)}{\partial \lambda^2} \qquad \text{(S6)}$$

The overwhelming contribution of the second derivative, whose amplitude is ten time larger than that of the first derivative (Eq. S6), shows that a permanent dipole change $\boldsymbol{m}_{0\mathrm{k}}$ caused by the electronic transition is dominant. This provides an evidence for the presence of a large number of CT excitons 2 ps after pulsed photoexcitation of the sample.

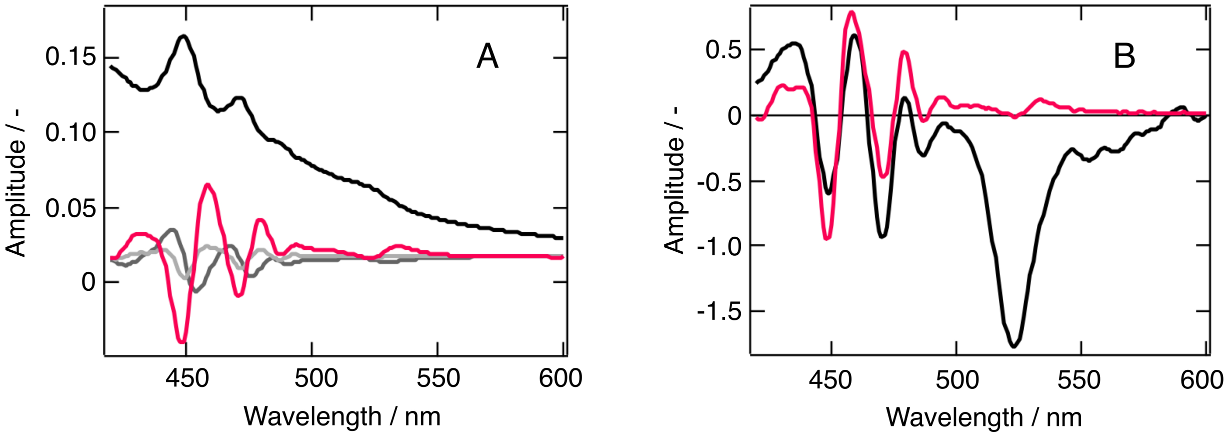

Fig. S3 A) Linear absorption spectrum of $CH_3NH_3PbBr_3$ nanoparticles (black line). The red line represents a linear combination (Eq. S6) of the calculated first derivative (dark grey line) and second derivative (light grey line) of the absorption spectrum. B) The transient absorption spectrum measured at a time delay of 2 ps (black line, λ_{ex}=390 nm, energy fluence = 9 μJ cm^{-2}) is best fitted with the differential spectrum calculated with Eq. S6 (red line).

S5. Photoemission quenching by donors in solution – Stern-Volmer plots

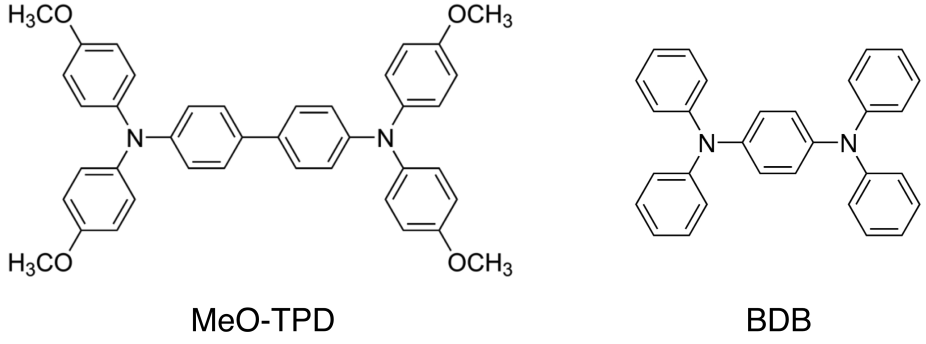

Fig. S4 Schematized molecular structures of the donor molecules N,N,N,N-tetrakis-(4-methoxyphenyl)benzidine (MeO-TPD) and 1,4-bis(diphenylamino)benzene (BDB).

The intensity of the photoemission of colloidal solutions of perovskite nanoparticles was measured for increasing concentrations of the donor molecules MeO-TPD and BDB. The photoemission is observed to be quenched efficiently for donor concentrations in the solution of the order of 10^{-4} mol L^{-1}. Figure S5 displays Stern-Volmer plots where the ratio I_0 / I of the intensity measured without and with the quencher present is plotted versus the quencher's concentration in solution.

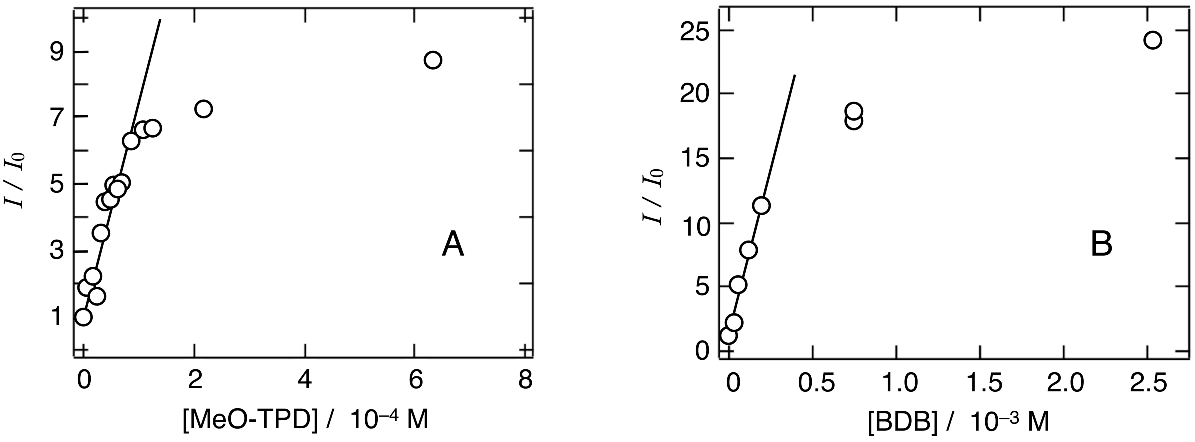

Fig. S5 Stern-Volmer plots for chlorobenzene solutions of $CH_3NH_3PbBr_3$ nanoparticles in presence of two different quenchers (λ_{em} = 520 nm) : MeO-TPD (A) and BDB (B).

Stern-Volmer plots obtained for the two redox quenchers display a linear portion at low concentrations. A significant deviation from the linearity and saturation of the quenching efficiency, however, is observed for [MeO-TPD] > 10^{-4} M and [BDB] > 3×10^{-4} M.

The slopes of the initial linear parts of the plots (Fig. S4) are estimated from a linear regression over the first points and yield values of the Stern-Volmer constant K_{SV}. This constant is defined as $K_{SV} = k_q \cdot \tau_0$, where k_q is the second order rate constant of the quenching process and τ_0 the photoemission lifetime in the absence of quencher.

Table 1 Stern-Volmer constants and quenching rate constants extracted from Stern-Volmer plots (Fig. S5). A value $\tau_0 \simeq 10^{-6}$ s provided by TCSPC measurements is considered for the photoemission lifetime.

	K_{SV} / L·mol^{-1}	k_q / L mol^{-1} s^{-1}
MeO-TPD	$6.3\times10^4 \pm 3.3\cdot10^3$	6×10^{10}
BDB	$5.3\times10^4 \pm 3.2\cdot10^3$	5×10^{10}

Approximate k_q values extracted from the Stern-Volmer plots appear to be larger than the second order rate constant for diffusion between capped nanoparticle aggregates and donor molecules in solution, which approximate value is estimated in our case at $k_{diff} \simeq 10^9$ L mol^{-1} s^{-1}. This therefore indicates that the quenching processes involving $CH_3NH_3PbBr_3$ nanoparticles takes place with donor molecules associated within the organic capping layer of the perovskite. This conclusion is also compatible with the observation of the saturation of the quenching process that, by comparison with the case of large MeO-TPD molecules, intervenes at higher concentrations for smaller BDB molecules.

A pseudo-first order reaction rate constant k_q' for electron transfer from a redox quencher, which concentration [Q] is considered practically constant during the reaction, to the perovskite valence band could be defined by $k_q' = k_q \cdot [Q]$. From the maximum concentration values observed within the linear portions [MeO-TPD] = 10^{-4} M and [BDB] = 3×10^{-4} M, one then derives $k_q = 6\times10^6$ s^{-1} and $k_q = 1.7\times10^7$ s^{-1}, which corresponds to time constants $\tau = 1/\ k_q$ of the order of 170 ns and 60 ns for the two donors MeO-TPD and BDB, respectively.

References

(1) Van Stokkum, I. H. M.; Larsen, D. S.; van Grondelle, R. Global and Target Analysis of Time-Resolved Spectra. *Biochim. Biophys. Acta Bioenerg.* **2004**, *1657*, 82–104.

(2) Berera, R.; van Grondelle, R.; Kennis, J. T. M. Ultrafast Transient Absorption Spectroscopy: Principles and Application to Photosynthetic Systems. *Photosynth. Res.* **2009**, *101*, 105–118.

(3) Paraecattil, A- A.; Risse-De Jonghe, J.; Pranculis, V.; Teuscher, J.; Moser, J.-E. Dynamics of Photocarrier Separation in $MAPbI_3$ Perovskite Multigrain Films under a Quasistatic Electric Field. *J. Phys. Chem. C* **2016**, *120*, 19595-19602.

(4) Lanzani, G. "The Photophysics Behind Photovoltaics and Photonics". Wiley-VCH; Weinheim, 2012.